Controlling particle transitions with weak periodic perturbations

Yan-Hong Qin,[1] Ling-Zheng Meng,[2] Xiao-Lin Li,[2] Guo-Guo Xin,[2,3] and Li-Chen Zhao[2,3,4,*]

[1]*School of Mathematics, South China University of Technology, Guangzhou 510640, China*
[2]*School of Physics, Northwest University, Xi'an 710127, China*
[3]*Peng Huanwu Center for Fundamental Theory, Xi'an 710127, China*
[4]*Shaanxi Key Laboratory for Theoretical Physics Frontiers, Xi'an 710127, China*

(Received 11 February 2022; revised 26 May 2022; accepted 11 July 2022; published 25 July 2022)

We investigate the particle transition dynamics in two-component Bose-Einstein condensates dominated by pair-particle transitions by introducing weak periodic perturbations to the initial states. We show that the transitions can be well controlled by varying the perturbation period while maintaining the external fields and nonlinear parameters during the transition process. In particular, there exists a critical period at which the transition efficiency is approximately 100%, with a numerical error of 0.72%. Analytic Akhmediev breather solutions and linear stability analyses show that modulation instability is the underlying mechanism for these transition dynamics. Furthermore, we establish a quantitative relation between the transition efficiency and phase shifts induced by the modulation instability. This relation can be used to measure the phase shift of the plane-wave background in well-known Akhmediev breathers.

DOI: 10.1103/PhysRevA.106.013318

I. INTRODUCTION

The experimental realization of the Bose-Einstein condensate (BEC) launched a new era in the investigation of particle transition dynamics between two quantum states due to its unique macroscopic and controllable properties [1–5]. Particle transition dynamics in two-component BECs and two-mode systems, including single-particle transition [6–18] and pair-particle transition effects [19–22], have been the main focus of research over the past two decades. For single-particle transitions (i.e., linear coupling), multiple types of particle transition dynamics have been demonstrated in BECs confined in double-well potentials (or other effective nonlinear two-level systems), such as nonlinear Josephson oscillations [6–8], nonlinear Rosen-Zener transition dynamics [9–12], and nonlinear Landau-Zener transitions [13–17]. Additional particle transition dynamics have been observed in other BEC systems trapped in periodic potentials [23,24] and other circumstances [25,26]. Highly controllable particle transitions are crucial for applications in atomic and molecular physics, such as high-precision measurements and quantum information processing [27–30].

Controllable particle transitions are usually realized by time-dependently manipulating the external fields or nonlinear parameters during the transition process [9,12–14,18]. These manipulations are essential for single-particle transition dynamics since particles tend to pass through the transition path if the particles do not occur in the self-trapping regime. Interestingly, particles may not pass through the transition path when pair-particle transitions dominate [19,22]. Some nonlinear effects can induce particle transitions in various circumstances, such as interference effects between different nonlinear waves and phase shifts induced by nonlinear wave collisions [20,21]. These characteristics suggest that there are many possibilities for controlling particle transition dynamics without manipulating the external fields or nonlinear parameters during the transition process when pair-particle transitions dominate.

This paper reports that controllable particle transition dynamics can be realized in two-component BECs with strong pair-particle transition effects by introducing a weak periodic perturbation to the initial states. The transition efficiency and transition time are investigated for various perturbation periods through direct numerical simulations. The results indicate that the desired final states can be achieved by adjusting the period of the initial perturbation rather than by manipulating the external fields or nonlinear parameters during the transition process. However, switch manipulation of the nonlinear strength is still necessary for the initial state operation. We achieve a nearly perfect particle transition with a transition efficiency of almost 100% with a specific perturbation period. Moreover, we provide analytic descriptions for the particle transition dynamics with exact Akhmediev breather solutions and linear stability analyses. Our analysis suggests that modulation instability is the generation mechanism of controllable particle transitions. The analytic descriptions are consistent with the numerical simulation results, except for perturbations with large periods. The complicated particle transition dynamics related to the initial perturbations with large periods can be explained by higher-order modulation instability. The analytic results provide a quantitative relation between the transition efficiency and the phase shift induced by the modulation instability, resulting in a potential method for measuring the background phase shift of the Akhmediev breather.

Our paper is organized as follows. In Sec. II, we present a theoretical model for two hyperfine states in the ^{87}Rb BEC with particle transition effects. In Sec. III, we use numerical

*zhaolichen3@nwu.edu.cn

simulations to demonstrate the highly controllable particle transition phenomena by manipulating initial weak perturbations. In addition, the transition efficiency and transition time are characterized in detail. Then, we present analytic descriptions for the transition dynamics. In Sec. IV, we demonstrate that modulation instability is the underlying mechanism of the particle transition dynamics. The analytic descriptions are consistent with the numerical simulation results, except for cases with large perturbation periods. In Sec. V, the complicated particle transition behavior of perturbations with large periods is explained by higher-order modulation instability. In Sec. VI, we propose an application of the particle transition phenomena for measuring the phase shift of the plane-wave background in Akhmediev breathers. In Sec. VII, we discuss the possibility of observing the transition dynamics in experiments. Finally, the conclusions are discussed in Sec. VIII.

II. PHYSICAL MODEL AND THEORETICAL CONCEPTS

We consider a two-component BEC with particle transition effects that is confined in a harmonic trapping potential. To reach a quasi-one-dimensional (quasi-1D) regime, highly anisotropic traps with axial and radial trapping frequencies that satisfy the condition $\omega_x \ll \omega_\perp$ are selected; thus, the radial characteristic length is less than the healing length, and the dynamics are essentially 1D [31]. The dimensionless mean-field energy functional for the (quasi-1D) two-component BEC system can be written as

$$E = \int_{-\infty}^{+\infty} \Big[\psi_1^* \Big(-\frac{1}{2}\partial_x^2 \Big) \psi_1 + \psi_2^* \Big(-\frac{1}{2}\partial_x^2 \Big) \psi_2 + g_{12}|\psi_1|^2|\psi_2|^2 + \frac{1}{2}g_{11}|\psi_1|^4 + \frac{1}{2}g_{22}|\psi_2|^4 + J_1(\psi_1^*\psi_2 + \psi_1\psi_2^*) + \frac{1}{2}J_2(\psi_1^{*2}\psi_2^2 + \psi_1^2\psi_2^{*2}) \Big] dx, \tag{1}$$

where x is the axial coordinate and the field ψ_1 (ψ_2) describes the wave function of the first (second) component.

The time evolution of the two-component BEC can be derived from the variational principle: $i\partial\psi_j/\partial t = \delta E/\delta\psi_j^*$ ($j = 1, 2$). We can substitute Eq. (1) into this formula to obtain the following dynamical equation:

$$i\begin{bmatrix}\psi_{1,t}\\ \psi_{2,t}\end{bmatrix} = \begin{bmatrix} H_1^0 + H_1^{MF} & J_1 + J_2\psi_1^*\psi_2 \\ J_1 + J_2\psi_1\psi_2^* & H_2^0 + H_2^{MF}\end{bmatrix}\begin{bmatrix}\psi_1\\ \psi_2\end{bmatrix}. \tag{2}$$

Here, $H_j^0 = -\frac{1}{2}\partial_x^2$, $H_1^{MF} = g_{11}|\psi_1|^2 + g_{12}|\psi_2|^2$, and $H_2^{MF} = g_{22}|\psi_2|^2 + g_{21}|\psi_1|^2$ are the mean field interactions. $g_{11} = g_{22}$ is the intracomponent interaction strength, and $g_{12} = g_{21}$ is the intercomponent interaction strength, which are characterized by the corresponding s-wave scattering lengths. J_1 and J_2 denote the first-order (single-particle) and second-order (pair-particle) atom transition strengths [4,5,8], respectively. The dimensionless form used in this work was obtained after a renormalization of the length $x' = \sqrt{\frac{\hbar}{m\omega_\perp}}x$, time $t' = t/\omega_\perp$, energy $E' = \hbar\omega_\perp E$, interatomic interactions coefficients $g'_{ij} = \sqrt{\frac{\hbar}{m\omega_\perp}}\hbar\omega_\perp g_{ij}$, $J'_2 = \sqrt{\frac{\hbar}{m\omega_\perp}}\hbar\omega_\perp J_2$, $J'_1 = \hbar\omega_\perp J_1$, and wave function $\psi'_j(x') = (\frac{m\omega_\perp}{\hbar})^{\frac{1}{4}}\psi_j(x)$. The transition terms can be realized by combining external coupling fields, such as radio frequency, microwave fields [32,33], and coupling sweeps (phase-transition sweeps) [34]. The experimental observations suggested that first-order tunneling could be highly suppressed, while second-order tunneling processes dominate in double-well potentials [4,5]. The two-mode tunneling dynamics are similar to the transition behavior of a two-component BEC [7–10]. It is naturally expected that the second-order transition term can dominate with proper nonlinear interactions. Furthermore, the first-order coherence vanished after the sweep, while the second-order coherence was macroscopically large under moderately rapid exponential sweeps [35,36]. Therefore, we consider the case when the second-order transition dominates, namely, $J_1 \ll J_2$. This case provides the possibility of controlling the particle transition dynamics without manipulating the external fields or nonlinear parameters during the transition process [19–22], in contrast to the cases guided by single-particle transitions [9,12–14,18], in which the external fields or nonlinear parameters must be controlled.

We study the particle transition dynamics in the coupled model shown in Eq. (2) with the system parameters $g_{12} = -2$, $g_{11} = g_{22} = J_2 = -1$, and $J_1 = -0.01$. For simplicity and without loss of generality, we assume that the atoms mainly populate one of the components. We introduce weak periodic perturbations to the two components simultaneously. These perturbations are induced by periodic external potentials by applying far off-resonant standing light waves or spatially periodic magnetic fields [37–39]. Then, the initial states are given as

$$\psi_1(x, t = 0) = 1 + \epsilon\cos\Big(\frac{2\pi}{D}x\Big), \tag{3a}$$

$$\psi_2(x, t = 0) = -\epsilon\cos\Big(\frac{2\pi}{D}x\Big). \tag{3b}$$

Here, D and ϵ ($\epsilon \ll 1$) are the period and amplitude of the periodic perturbation, respectively. It should be mentioned that these initial states are not the solution of the dynamical equation [Eq. (2)] and are not stable; however, they can first be prepared by setting the nonlinear parameters in the repulsive interaction regime according to quantum engineering techniques [40–42]. Then, we manipulate the nonlinear parameters in several microseconds by using the Feshbach resonance to switch the atomic interactions from repulsive to attractive [43–45]. The two states will evolve and redistribute in several milliseconds due to modulation instability. During this process, we no longer need to manipulate the nonlinear parameters and external potentials. This is discussed in detail in Sec. VII. The basic particle transition schematic diagram is shown in Fig. 1. Due to the emergence of single-particle and pair-particle transition effects, Eq. (2) can no longer be solved analytically. Therefore, we exploit the fourth-order Runge-Kutta algorithm to numerically trace its evolution. We are concerned with the population evolution of each component during the particle transition process. The population $N_j = \int |\psi_j|^2 dx$ ($j = 1, 2$) should be calculated in the integration interval $[-nD, nD]$ (where n is a positive integer), with n adjusted for different periods D.

It is appropriate to characterize the particle transition process using the variation in the relative population (RP)

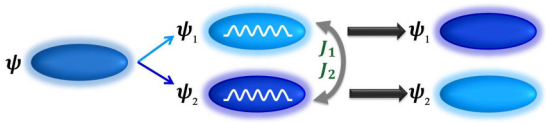

FIG. 1. Sketch of particle transition between two hyperfine states of ^{87}Rb condensates with hyperfine states ψ_1 and ψ_2. J_1 and J_2 denote the first-order (single-particle) and second-order (pair-particle) atom transition strengths. When $J_2 \gg J_1$ and both components are simultaneously subjected to weak periodic perturbations, particle transitions can occur between two states.

between the two components. The RP herein is defined as

$$\eta(t) = \frac{N_1 - N_2}{N_1 + N_2}. \tag{4}$$

Since the perturbations applied to the initial states in Eq. (3) are very weak, the initial RP $\eta(0)$ can reasonably be regarded as 1. Therefore, the transition efficiency can be determined according to the RP difference $\Delta\eta$ between the initial and final states, namely,

$$\Delta\eta = 1 - \eta(t). \tag{5}$$

A larger value of $\Delta\eta$ results in a higher transition efficiency. Notably, $\Delta\eta = 0$ and $\Delta\eta = 2$ correspond to transition efficiencies of 0% and 100%, respectively. Next, we use $\Delta\eta$ to quantitatively characterize the transition efficiency.

III. PARTICLE TRANSITION DYNAMICS INDUCED BY WEAK PERIODIC PERTURBATIONS

A. Numerical simulation results

Our numerical simulations indicate that particle transitions can be well driven by the weak periodic perturbations, while keeping the nonlinear parameters and transition terms unchanged during the transition process. A typical particle transition phenomenon is presented in Fig. 2, with $D = \sqrt{2}\pi$

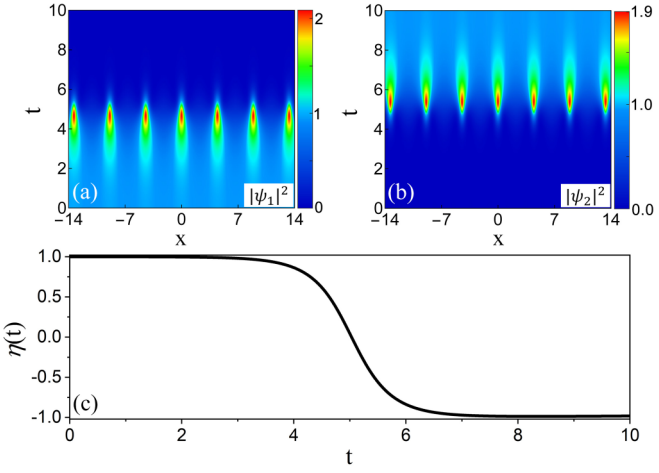

FIG. 2. An approximate 100% population transfer between the two components. (a) and (b) correspond to the density evolutions of components ψ_1 and ψ_2, respectively. (c) Numerical results of RP versus time. The RP of the initial and final states is flipped. The parameters are $D = \sqrt{2}\pi$ and $\epsilon = 0.0095$.

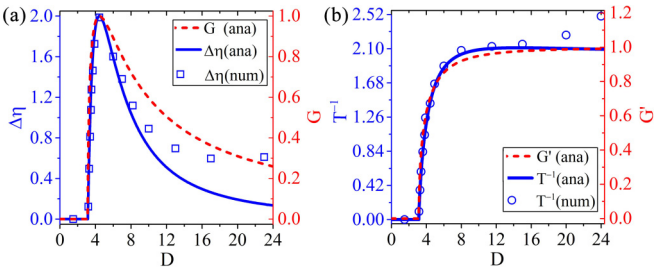

FIG. 3. (a) The RP difference $\Delta\eta$ and the modulation instability gain G versus the perturbation period D. The blue squares and blue solid curve correspond to the numerical and analytical results, respectively. The red dashed line represents the modulation instability gain. The transition efficiency is proportional to the modulation instability gain G over a large range of perturbation periods. (b) The inverse of the transition time T^{-1} and the other modulation instability gain G' versus the perturbation period D. The blue circles and blue solid curve correspond to the numerical and analytical results, respectively. The red dashed line represents the other modulation instability gain G'. The results show that T^{-1} and G' have the same change trend with the period. However, the simulation results deviate from the analytical results for the perturbation with a large period due to higher-order modulation instability.

and $\epsilon = 0.0095$. Figures 2(a) and 2(b) correspond to the density evolutions of components ψ_1 and ψ_2, respectively. At approximately $t = 5$, periodic breathing structures appear in the spatial direction for both components, which are similar to the well-known Akhmediev breather [46,47]. However, the background density of each component varies greatly after the emergence of the breathing structure, resulting in a large number of particles transferring from component ψ_1 to component ψ_2. To further describe the particle transition process, we show the RP evolution in Fig. 2(c), which presents three distinct transition stages. In the first stage ($0 < t \lesssim 3$), the RP remains almost unchanged; namely, a small fraction of particles is transferred from component ψ_1 to component ψ_2. In the middle stage ($3 < t \lesssim 7$), the RP changes from approximately 1 to -1. This result signifies sharp and rapid particle transitions between the two components, and the breather structures form during this period. In the final stage ($t > 7$), the RP gradually stabilized, with a value of approximately -1. This value indicates a nearly perfect particle transition between the two components, achieving a transition efficiency of nearly 100% with a numerical error of only 0.72%.

Furthermore, we discuss the relations between the transition efficiency and the initial perturbation period. The numerical results are shown in Fig. 3(a) as blue squares. The perturbation period has four distinct intervals. (i) When $0 < D \leqslant \pi$, $\Delta\eta$ is zero, indicating that no particle transitions occur between the two components. (ii) When $\pi < D \leqslant \sqrt{2}\pi$, the transition efficiency improves significantly with increasing perturbation period. In particular, when D equals $\sqrt{2}\pi$, the transition efficiency reaches nearly 100%; that is, the production of the particle transition is maximized. (iii) When $\sqrt{2}\pi < D < 16$, the transition efficiency decreases with increasing perturbation period. (iv) When $D \geqslant 16$, the transition efficiency anomalously increases with increasing perturbation period. These numerical results demonstrate that particle

transitions can be controlled by the initial periodic perturbation, providing a possible way to control particle transition dynamics without manipulating the external fields or nonlinear parameters during the transition process.

The transition time of the particle transition process has also attracted considerable attention [48–51]. In a nonlinear Landau-Zener model, the transition time indicates the amount of time in which the system experiences a structural change that leads to a nonzero transition probability in the adiabatic limit [51]. Thus, we also investigated the time to complete the particle transition process for different initial modulation periods. First, we define an appropriate quantity to characterize the particle transition time. Because breatherlike density distributions appear at a certain time during the particle transition process, we define the transition time as $T = |T_1 - T_2|$, where $T_j (j = 1, 2)$ denotes the time when the density of the breathing structure reaches a maximum in each component. The variations in T with the initial perturbation period are numerically shown in Fig. 3(b) (see the blue circles), where T^{-1} is the inverse of T. The transition time T first decreases (T^{-1} increases; $D < 10$) and then remains approximately constant with increasing perturbation period ($10 \leqslant D < 16$). However, the transition time decreases (T^{-1} increases) when $D \geqslant 16$, which is explained in detail in Sec. V.

B. Analytical descriptions of the transition dynamics

We would like to derive an analytical description of the above particle transition dynamics to comprehensively analyze the transition characteristics. Since the pair transition guides the particle transition between the two components, we can investigate the transition dynamics with an integrable coupled nonlinear Schrödinger equation with a pair-transition term [52] while safely ignoring the single-particle transition effect (i.e., $J_1 = 0$). Our simulation results demonstrate Akhmediev breatherlike structures during the particle transition (see Fig. 2). Akhmediev breathers can be excited by superimposing weak periodic perturbations on plane-wave backgrounds [46,53]. Thus, we analytically derive the Akhmediev breather solutions of the integrable model, which can be expressed as [19,22]

$$\psi_1 = \frac{1}{2}e^{it}\left[1 + \frac{a\cos(\omega x) - \sigma\cosh(\delta t) + i\delta\sinh(\delta t)}{a\cos(\omega x) - \cosh(\delta t)}e^{i\tau}\right],$$
$$\psi_2 = \frac{1}{2}e^{it}\left[1 - \frac{a\cos(\omega x) - \sigma\cosh(\delta t) + i\delta\sinh(\delta t)}{a\cos(\omega x) - \cosh(\delta t)}e^{i\tau}\right], \tag{6}$$

where $\sigma = 2a^2 - 1$, $\omega = 2\sqrt{1-a^2}$, $\delta = a\omega$, and $a = \frac{\sqrt{D^2-\pi^2}}{D}$. The parameter D is the spatial period and satisfies $D > \pi$ for this breather solution. The parameter τ is a real constant that can be used to adjust the initial phase of the solution. The second term on the right-hand side of Eq. (6) is identical to the well-known Akhmediev breather solution of the scalar nonlinear Schrödinger equation [46].

To analytically analyze the above numerical simulations, we first ensure that $\eta(0) = 1$ at the initial states for a perturbation with an arbitrary period. We deduce the asymptotic expressions of Eq. (6) in the limit of $t \to \mp\infty$ to describe the initial state (ψ_j^i) and final state (ψ_j^f) of the breather solution. When $t \to -\infty$, we obtain $\psi_1^i = \frac{1}{2}e^{it}[1 + e^{i(\tau+\varphi^i)}]$ and $\psi_2^i = \frac{1}{2}e^{it}[1 - e^{i(\tau+\varphi^i)}]$, where φ^i is the phase of the complex number $\sigma + i\delta$. We maintain $|\psi_1^i|^2 = 1$ and $|\psi_2^i|^2 = 0$ by setting $\tau = -\varphi^i$ so that $\eta(0) = 1$ is satisfied in the analytical analyses. When $t \to +\infty$, the asymptotic expressions of the final states of Eq. (6) are $\psi_1^f = \frac{1}{2}e^{it}[1 + e^{i(\tau+\varphi^f)}]$ and $\psi_2^f = \frac{1}{2}e^{it}[1 - e^{i(\tau+\varphi^f)}]$, where φ^f is the phase of the complex number $\sigma - i\delta$. The exact forms of φ^i and φ^f for various perturbation periods are summarized in Table I. It is easy to obtain $|\psi_1^f|^2 = \cos[\frac{\varphi^i-\varphi^f}{2}]^2$, $|\psi_2^f|^2 = \sin[\frac{\varphi^i-\varphi^f}{2}]^2$. Therefore, the RP of the final state can be calculated as $\eta(t) = \cos(\Delta\varphi)$, where $\Delta\varphi = \varphi^f - \varphi^i$. In fact, $\Delta\varphi$ corresponds to the phase shift of the plane-wave background in the Akhmediev breather. Consequently, the RP difference between the initial and final states can be analytically expressed as

$$\Delta\eta = 1 - \cos(\Delta\varphi). \tag{7}$$

TABLE I. The initial phase and final phase of the Akhmediev breather's background in different periods.

Period D	Initial phase φ^i	Final phase φ^f
$(\pi, \sqrt{2}\pi)$	$\arctan[\delta/\sigma] + \pi$	$-\arctan[\delta/\sigma] - \pi$
$\sqrt{2}\pi$	$\pi/2$	$3\pi/2$
$(\sqrt{2}\pi, +\infty)$	$\arctan[\delta/\sigma]$	$-\arctan[\delta/\sigma]$

The analytical results based on Eq. (7) are shown by the blue solid curve in Fig. 3(a). The results agree well with the numerical results (blue squares) for a large range of initial-state periods. Then, the transition time can be calculated analytically as $T = |T_1 - T_2|$, where T_j can be obtained exactly by determining the roots of $\partial_t|\psi_j(x = 0)|^2 = 0$ ($j = 1, 2$). The corresponding analytical results of T^{-1} are shown by the blue solid curve in Fig. 3(b), and the results also agree with the numerical results (blue circles) for a certain range of periods. However, for perturbations with large periods, the numerical results deviate from the analytical results, which will be discussed in Sec. V.

The good agreement between the analytical and numerical results indicates that the Akhmediev breather solutions can characterize the particle transition process. It is well known that the Akhmediev breather solution can describe the modulation instability characteristics of a plane-wave background [46,54]. The initial stage in the development of the modulation instability was investigated with the linearization method [55–57]. Therefore, the modulation instability of a two-component BEC with particle transition effects could help to explain these transition dynamics.

IV. MECHANISM FOR THE PARTICLE TRANSITION DYNAMICS

We perform a standard linear instability analysis by adding small-amplitude Fourier modes to the initial backgrounds of Eq. (3), namely, $\psi_1 = (1 + f_+e^{i\kappa(x-\Omega t)} + f_-e^{-i\kappa(x-\Omega t)})e^{it}$,

$\psi_2 = (0 + g_+ e^{i\kappa(x-\Omega t)} + g_- e^{-i\kappa(x-\Omega t)})e^{it}$ (where $f_\pm$ and $g_\pm$ are the small amplitudes of the Fourier modes). After these values are substituted into Eq. (2) with $J_1 = 0$, the equations are linearized, and we obtain the following dispersion relation: $\Omega = \pm\frac{1}{2}\sqrt{\kappa^2 - 4}$, where $\kappa = \frac{2\pi}{D}$. Then, the modulation instability gain can be expressed as $G = \mathrm{Im}|\kappa\Omega|$. Although this expression is mathematically precise, it cannot reasonably demonstrate the modulation instability gain value near the resonance line $\kappa = 0$ (i.e., $D \to \infty$) [57]. It should be noted that the modulation instability gain has another form, namely, $G' = \mathrm{Im}|\Omega|$. This gain properly reflects the modulation instability growth rate in physics since the growth rate tends to reach its maximum value on the resonance line in this form.

The modulation instability gain G versus the perturbation period D is demonstrated by the red dashed curve in Fig. 3(a). The modulation instability gain has the same change trend as the analytical RP difference results. When $0 < D \leqslant \pi$, the modulation instability gain is zero, and the RP difference is also equal to zero. This result indicates that there are no particle transitions between the two components in the absence of modulation instability. When $D > \pi$, the modulation instability gain is stronger, and more particles are transferred from component ψ_1 to component ψ_2. In particular, when the perturbation period is equal to $\sqrt{2}\pi$, the modulation instability gain reaches its maximum value of 1, and the transition efficiency achieves its highest value of 100%. On the other hand, we note that the other form of the modulation instability gain, $G' = \mathrm{Im}|\Omega|$, has the same trend as the transition time for different perturbation periods, as shown in Fig. 3(b) by the red dashed curve. These results suggest that the modulation instability can be used to understand the generation mechanism of particle transition dynamics. This differs significantly from the Bloch-band tunneling reported in [24], in which the tunneling dynamics strongly depend on the band gap structure and modulation instability.

We emphasize that the numerical simulation results deviate from the analytical results when the perturbation period is substantially larger. These deviations occur because higher-order modulation instability arises when the perturbation period exceeds 2π [58]. The higher-order modulation instability causes complex dynamics after the first particle transition. In the following section, we investigate the particle transition dynamics for initial perturbations with large periods in detail.

V. COMPLICATED PARTICLE TRANSITION DYNAMICS WITH HIGHER-ORDER MODULATION INSTABILITY

Based on the quantitative relations between the modulation instability and the nonlinear excitations [57], when the perturbation period is less than 2π, a fundamental particle transition is induced by the fundamental modulation instability. However, when the perturbation period is in the range of $D > 2\pi$, higher-order modulation instability induces particle transitions with complex splitting dynamics [58]. The higher-order modulation instability effect becomes more noticeable for perturbations with considerably larger periods. Our simulation results show that complex splitting dynamics can lead to large deviations from the analytic descriptions, as shown in Fig. 3 for $D > 16$.

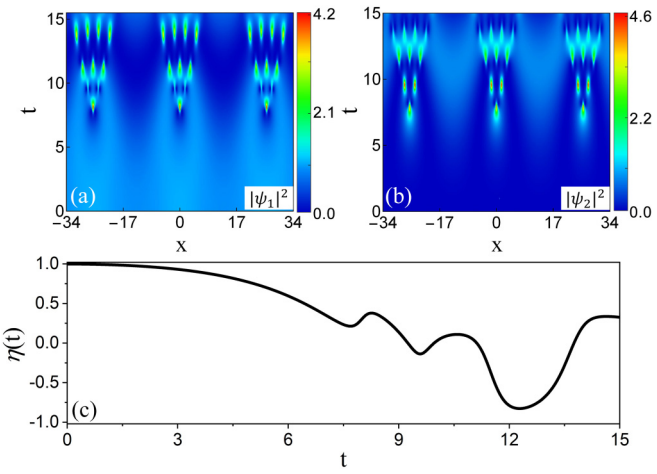

FIG. 4. Complicated particle transition dynamics for initial perturbations with large periods. (a) and (b) correspond to components ψ_1 and ψ_2, respectively. The simulation results show complex splitting dynamics induced by the higher-order modulation instability. (c) The time evolution of RP. The parameters are $D = 26$ and $\epsilon = 0.033$.

For example, we show the numerical results with a perturbation period of $D = 26$ in Fig. 4. The results present complicated particle transition dynamics, in sharp contrast to the fundamental particle transition shown in Fig. 2. The simulations show a series of progressive spatial bifurcation dynamics induced by higher-order modulation instability. These excitations split the initial modulated field into up to four subwaves during the evolution. Similar phenomena have been shown both numerically and experimentally in scalar nonlinear systems [58–60]. We present the corresponding evolution of the RP in Fig. 4(c). The result demonstrates that the RP changes dramatically over time due to the splitting dynamics, resulting in deviations from the analytical descriptions.

VI. APPLICATION OF PARTICLE TRANSITION DYNAMICS

The background phase shift $\Delta\varphi$ of the Akhmediev breather solution is directly related to the transition efficiency for a certain perturbation period [see Eq. (5)]. This result indicates that the phase shift can be represented in the following form:

$$\Delta\varphi = \pm\arccos(1 - \Delta\eta). \tag{8}$$

We plot the relation between the phase shift and the transition efficiency in Fig. 5. Here, we show only the positive branch of the phase shift, as the negative branch has a distribution symmetric to the positive branch. A phase shift of zero cannot induce particle transitions, while a phase shift of π results in the maximum number of particle transitions. It should be noted that because Kuznetsov-Ma breathers and rogue waves do not have global phase shifts between the final and initial states, they can experience only local particle transitions, and thus, the particles eventually return to their original component [19,22]. These results suggest that the background phase shift of the Akhmediev breather plays a crucial role in particle transition dynamics. This characteristic is helpful for

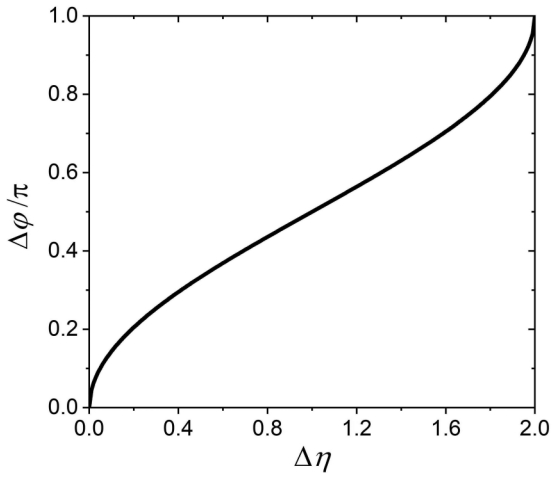

FIG. 5. The phase shift $\Delta\varphi$ of the plane-wave background of the Akhmediev breather versus the transition efficiency $\Delta\eta$.

understanding the two modulation-instability-gain forms shown in Fig. 3.

More importantly, the quantitative phase-shift relation shown in Eq. (8) is meaningful for measuring the nonlinear phase shift of the well-known Akhmediev breather based on the transition efficiency. A perturbation with a trigonometric function form has been widely used to excite Akhmediev breathers both numerically and experimentally [58,61,62]. Therefore, this relation offers a potential new method for measuring the phase shift of the breather's plane-wave background.

VII. POSSIBILITIES FOR OBSERVING THE PARTICLE TRANSITION DYNAMICS

We discuss the possibility of observing particle transition dynamics in a two-component BEC. We consider two hyperfine states, $|F=1, m_F=-1\rangle = |\psi_1\rangle$ and $|F=2, m_F=1\rangle = |\psi_2\rangle$, in the ^{87}Rb BEC trapped by the harmonic potential $\frac{1}{2}\omega_\perp^2(y^2+z^2)+\frac{1}{2}\omega_x^2x^2$ [41,42,63]. The atoms mainly populate state $|\psi_1\rangle$, while state $|\psi_2\rangle$ is coupled to $|\psi_1\rangle$ through the radio frequency or microwave-pulse or sweep techniques [32–34,41,63]. These techniques can also be utilized to ensure that pair-particle transitions dominate [34]. The Feshbach resonance or confinement-induced resonance is used to ensure that the nonlinear interaction strength satisfies our condition [64–66]. The evolution of the particle transition in the three-dimensional (3D) setting can be described by $i\psi_{1,t} = -\frac{1}{2}\nabla^2\psi_1+(g_{11}^{3D}|\psi_1|^2+g_{12}^{3D}|\psi_2|^2)\psi_1+J_1\psi_2+J_2^{3D}\psi_2^2\psi_1^*+[\omega_\perp^2(y^2+z^2)/2+\omega_x^2x^2/2]\psi_1$ and $i\psi_{2,t} = -\frac{1}{2}\nabla^2\psi_2+(g_{22}^{3D}|\psi_2|^2+g_{12}^{3D}|\psi_1|^2)\psi_2+J_1\psi_1+J_2^{3D}\psi_1^2\psi_2^*+[\omega_\perp^2(y^2+z^2)/2+\omega_x^2x^2/2]\psi_2$, where $g_{ij}^{3D}=\frac{2\pi}{\omega_\perp}g_{ij}$ and $J_2^{3D}=\frac{2\pi}{\omega_\perp}J_2$, and the atomic mass and Planck's constant are rescaled to 1. The other parameters are the same as those in the homogeneous case.

We first prepare the initial states by setting the nonlinear parameters in the repulsive interaction regime since the background of the breather excitation is not stable in the attractive interaction case, which makes it difficult to prepare the initial states for the above transition dynamics.

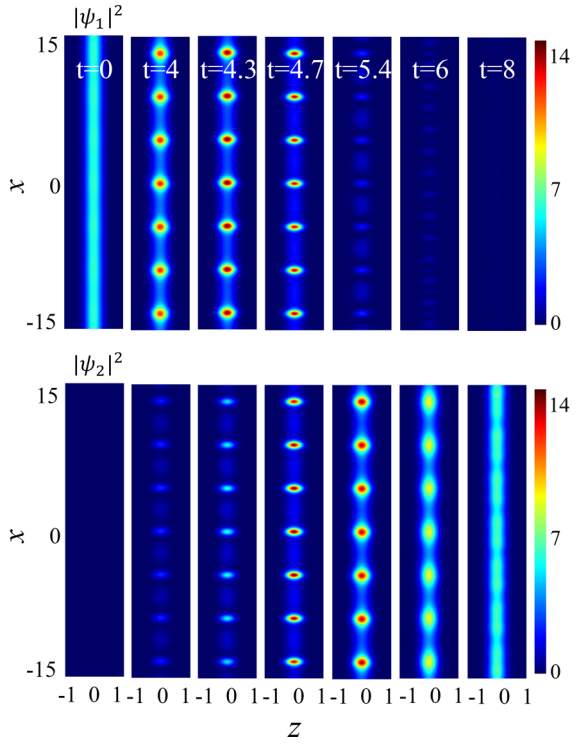

FIG. 6. The particle transition dynamics in a 3D setting with a harmonic trap along the x axis ($\omega_x=0.01$ and $\omega_\perp=20$). The dynamics agree well with the effective 1D counterpart [see Figs. 2(a) and 2(b)]. Because the condensate has rotational symmetry along the x axis, only the x-z cross section is shown. The other parameters are the same as those in Fig. 2.

For repulsive interactions, we use a strongly confining transverse frequency $\omega_\perp$ and a weak axial frequency ω_x to ensure that the radial characteristic length is smaller than the healing length in the quasi-1D approximation. Thus, the initial states of the numerical evolutions are $\psi_1=[1+\epsilon\cos(\frac{2\pi}{D}x)]\sqrt{\max((1-\omega_x^2x^2/2)/|g_{11}|,0)}\sqrt{\frac{\omega_\perp}{\pi}}e^{-\frac{1}{2}\omega_\perp(y^2+z^2)}$ and $\psi_2=-\epsilon\cos(\frac{2\pi}{D}x)\sqrt{\max((1-\omega_x^2x^2/2)/|g_{22}|,0)}\sqrt{\frac{\omega_\perp}{\pi}}e^{-\frac{1}{2}\omega_\perp(y^2+z^2)}$, and the Thomas-Fermi ground state was used to modify the initial-state profiles. A considerably weaker harmonic trap along the x direction can be used to approximate the above initial states, as shown in Eq. (3) for the homogeneous case. The weak spatial external periodic potentials are temporarily and synchronously applied to the two states, producing periodic perturbations in each component by using a far-off-resonant laser field or a spatially periodic magnetic field [37–39].

Then, we switch the nonlinear parameters to the attractive interaction regime in several microseconds [43–45]. The transition dynamics in the 3D setting can be investigated in several milliseconds [40–44,63,67]. For example, we consider a BEC trapped in a harmonic potential with $\omega_\perp=20$ and $\omega_x=0.01$ (the radial characteristic length is approximately 0.22, and the healing length is approximately 0.71 in this case). We numerically solve the corresponding dynamical equation with the fourth-order integrating-factor method, and we apply periodic boundary conditions to both components because the

condensate is trapped. We show the transition dynamics in the axial range of $[-15, 15]$ in Fig. 6, which presents a striking particle transition phenomenon, the dynamics of which agree well with the effective 1D counterpart, as shown in Fig. 2.

In recent experiments, various types of vector solitons and breathers were successfully created in different BEC systems with well-developed quantum engineering techniques [40–42,63,67]. These results indicate that the initial states can be prepared in various forms in BEC systems [39,64–66,68], for which the operation time (several microseconds) of the initial states is substantially smaller than the characteristic evolution timescale (milliseconds for usual BECs) [40–42,63,67]. Our numerical simulations indicate that particle transition dynamics can emerge in 3D settings. This result provides many possibilities for observing controllable particle transition processes.

VIII. CONCLUSION AND DISCUSSION

We demonstrated that controllable particle transition dynamics can be obtained by introducing weak periodic perturbations to initial states in two-component BECs dominated by pair-particle transition effects. The detailed analyses revealed that modulation instability is the underlying mechanism of such transition dynamics. Additionally, we demonstrated the complicated particle transition dynamics for perturbations with spatial periods in the range of $D > 2\pi$, which are induced by higher-order modulation instability. This result suggests that controllable particle transitions should be realized outside the range of higher-order modulation instability. Furthermore, we proposed that the transition efficiency can be used to measure the background phase shift of Akhmediev breathers [47], which could be helpful for measuring the geometric phases of some nonlinear waves [69]. Our numerical simulations and recent experimental techniques [40–42,63–67] suggest that there are many possibilities for realizing the controllable particle transition.

ACKNOWLEDGMENTS

Y.-H.Q. was supported by the China Postdoctoral Science Foundation (Contract No. 2021M701255) and the National Natural Science Foundation of China (Contract No. 12147170). L.-C.Z. was supported by the National Natural Science Foundation of China (Contracts No. 12022513 and No. 11775176) and the Major Basic Research Program of Natural Science of Shaanxi Province (Grant No. 2018KJXX-094).

[1] M. R. Matthews, B. P. Anderson, P. C. Haljan, D. S. Hall, M. J. Holland, J. E. Williams, C. E. Wieman, and E. A. Cornell, Watching a Superfluid Untwist Itself: Recurrence of Rabi Oscillations in a Bose-Einstein Condensate, Phys. Rev. Lett. **83**, 3358 (1999).

[2] M. Albiez, R. Gati, J. Fölling, S. Hunsmann, M. Cristiani, and M. K. Oberthaler, Direct Observation of Tunneling and Nonlinear Self-Trapping in a Single Bosonic Josephson Junction, Phys. Rev. Lett. **95**, 010402 (2005).

[3] L. D. Carr, M. J. Holland, and B. A. Malomed, Macroscopic quantum tunnelling of Bose-Einstein condensates in a finite potential well, J. Phys. B **38**, 3217 (2005).

[4] S. Fölling, S. Trotzky, P. Cheinet, M. Feld, R. Saers, A. Widera, T. Müller, and I. Bloch, Direct observation of second-order atom tunnelling, Nature (London) **448**, 1029 (2007).

[5] S. Zöllner, H.-D. Meyer, and P. Schmelcher, Few-Boson Dynamics in Double Wells: From Single-Atom to Correlated Pair Tunneling, Phys. Rev. Lett. **100**, 040401 (2008).

[6] L. Fu and J. Liu, Quantum entanglement manifestation of transition to nonlinear self-trapping for Bose-Einstein condensates in a symmetric double well, Phys. Rev. A **74**, 063614 (2006).

[7] S. Raghavan, A. Smerzi, S. Fantoni, and S. R. Shenoy, Coherent oscillations between two weakly coupled Bose-Einstein condensates: Josephson effects, π oscillations, and macroscopic quantum self-trapping, Phys. Rev. A **59**, 620 (1999).

[8] J. Williams, R. Walser, J. Cooper, E. Cornell, and M. Holland, Nonlinear Josephson-type oscillations of a driven, two-component Bose-Einstein condensate, Phys. Rev. A **59**, R31(R) (1999).

[9] S. C. Li, L. B. Fu, W. S. Duan, and J. Liu, Nonlinear Ramsey interferometry with Rosen-Zener pulses on a two-component Bose-Einstein condensate, Phys. Rev. A **78**, 063621 (2008).

[10] X. Jiang, W. Duan, S. Li, and Y. Shi, Rosen-Zener transition of two-component Bose-Einstein condensates, J. Phys. B **42**, 185001 (2009).

[11] L.-C. Zhao, G. G. Xin, and Z. Y. Yang, Transition dynamics of a bright soliton in a binary Bose-Einstein condensate, J. Opt. Soc. Am. B **34**, 2569 (2017).

[12] D. F. Ye, L. B. Fu, and J. Liu, Rosen-Zener transition in a nonlinear two-level system, Phys. Rev. A **77**, 013402 (2008).

[13] B. Wu and Q. Niu, Nonlinear Landau-Zener tunneling, Phys. Rev. A **61**, 023402 (2000).

[14] J. Liu, L. Fu, B. Y. Ou, S. G. Chen, D. I. Choi, B. Wu, and Q. Niu, Theory of nonlinear Landau-Zener tunneling, Phys. Rev. A **66**, 023404 (2002).

[15] F. Q. Dou, S. C. Li, and H. Cao, Combined effects of particle interaction and nonlinear sweep on Landau-Zener transition, Phys. Lett. A **376**, 51 (2011).

[16] V. Loladze and R. Khomeriki, Landau-Zener tunneling of solitons, Phys. Rev. E **95**, 042204 (2017).

[17] A. Maroufian and M. Hosseini, The investigation of Landau-Zener transition in coupled three-particle systems, Optik **201**, 163520 (2020).

[18] F.-Q. Dou, Z.-M. Yan, and L.-N. Hu, Accurate control quantum transition in a nonlinear two-level system, Physica A **533**, 121932 (2019).

[19] L.-C. Zhao, L. Ling, Z.-Y. Yang, and J. Liu, Pair-tunneling induced localized waves in a vector nonlinear Schrödinger

equation, Commun. Nonlinear Sci. Numer. Simul. **23**, 21 (2015).
[20] Y.-H. Qin, L.-C. Zhao, Z.-Y. Yang, and W.-L. Yang, Several localized waves induced by linear interference between a nonlinear plane wave and bright solitons, Chaos **28**, 013111 (2018).
[21] L.-Z. Meng, Y.-H. Qin, L.-C. Zhao, and Z.-Y. Yang, Domain walls and their interactions in a two-component Bose-Einstein condensate, Chin. Phys. B **28**, 060502 (2019).
[22] L. Ling and L.-C. Zhao, Integrable pair-transition-coupled nonlinear Schrödinger equations, Phys. Rev. E **92**, 022924 (2015).
[23] M. Jona-Lasinio, O. Morsch, M. Cristiani, N. Malossi, J. H. Müller, E. Courtade, M. Anderlini, and E. Arimondo, Asymmetric Landau-Zener Tunneling in a Periodic Potential, Phys. Rev. Lett. **91**, 230406 (2003).
[24] V. A. Brazhnyi, V. V. Konotop, and V. Kuzmiak, Nature of the Intrinsic Relation between Bloch-Band Tunneling and Modulational Instability, Phys. Rev. Lett. **96**, 150402 (2006).
[25] G. Aydındoğan and K. Güven, Asymmetric Rosen-Zener-like transition through a soliton-surface-plasmon photonic Josephson junction with spatially varying coupling, Phys. Rev. A **96**, 053802 (2017).
[26] X. Xu, Z. Zhang, and Z. Liang, Nonequilibrium Landau-Zener tunneling in exciton-polariton condensates, Phys. Rev. A **102**, 033317 (2020).
[27] K. Bergmann, H. Theuer, and B. W. Shore, Coherent population transfer among quantum states of atoms and molecules, Rev. Mod. Phys. **70**, 1003 (1998).
[28] H. J. Kimble, The quantum internet, Nature (London) **453**, 1023 (2008).
[29] C. Brif, R. Chakrabarti, and H. Rabitz, Control of quantum phenomena: Past, present and future, New J. Phys. **12**, 075008 (2010).
[30] N. V. Vitanov, Relations between the single-pass and double-pass transition probabilities in quantum systems with two and three states, Phys. Rev. A **97**, 053409 (2018).
[31] P. G. Kevrekidis, D. J. Frantzeskakis, and R. Carretero-Gonzalez, *Emergent Nonlinear Phenomena in Bose-Einstein Condensates: Theory and Experiment* (Springer, Berlin, 2008).
[32] R. J. Ballagh, K. Burnett, and T. F. Scott, Theory of an Output Coupler for Bose-Einstein Condensed Atoms, Phys. Rev. Lett. **78**, 1607 (1997).
[33] M. R. Matthews, D. S. Hall, D. S. Jin, J. R. Ensher, C. E. Wieman, E. A. Cornell, F. Dalfovo, C. Minniti, and S. Stringari, Dynamical Response of a Bose-Einstein Condensate to a Discontinuous Change in Internal State, Phys. Rev. Lett. **81**, 243 (1998).
[34] J. Dziarmaga, Dynamics of a quantum phase transition and relaxation to a steady state, Adv. Phys. **59**, 1063 (2010).
[35] P. Bader and U. R. Fischer, Fragmented Many-Body Ground States for Scalar Bosons in a Single Trap, Phys. Rev. Lett. **103**, 060402 (2009).
[36] U. R. Fischer, K. S. Lee, and B. Xiong, Emergence of a new pair-coherent phase in many-body quenches of repulsive bosons, Phys. Rev. A **84**, 011604(R) (2011).
[37] B. Eiermann, P. Treutlein, Th. Anker, M. Albiez, M. Taglieber, K.-P. Marzlin, and M. K. Oberthaler, Dispersion Management for Atomic Matter Waves, Phys. Rev. Lett. **91**, 060402 (2003).
[38] B. Eiermann, Th. Anker, M. Albiez, M. Taglieber, P. Treutlein, K.-P. Marzlin, and M. K. Oberthaler, Bright Bose-Einstein Gap Solitons of Atoms with Repulsive Interaction, Phys. Rev. Lett. **92**, 230401 (2004).
[39] K. Henderson, C. Ryu, C. MacCormick, and M. G. Boshier, Experimental demonstration of painting arbitrary and dynamic potentials for Bose-Einstein condensates, New J. Phys. **11**, 043030 (2009).
[40] X. Chai, D. Lao, K. Fujimoto, R. Hamazaki, M. Ueda, and C. Raman, Magnetic Solitons in a Spin-1 Bose-Einstein Condensate, Phys. Rev. Lett. **125**, 030402 (2020).
[41] C. Becker, S. Stellmer, P. Soltan-Panahi, S. Dörscher, M. Baumert, E.-M. Richter, J. Kronjäger, K. Bongs, and K. Sengstock, Oscillations and interactions of dark and dark-bright solitons in Bose-Einstein condensates, Nat. Phys. **4**, 496 (2008).
[42] S. Lannig, C.-M. Schmied, M. Prüfer, P. Kunkel, R. Strohmaier, H. Strobel, T. Gasenzer, P. G. Kevrekidis, and M. K. Oberthaler, Collisions of Three-Component Vector Solitons in Bose-Einstein Condensates, Phys. Rev. Lett. **125**, 170401 (2020).
[43] L. Khaykovich, F. Schreck, G. Ferrari, T. Bourdel, J. Cubizolles, L. D. Carr, Y. Castin, and C. Salomon, Formation of a matter-wave bright soliton, Science **296**, 1290 (2002).
[44] S. L. Cornish, S. T. Thompson, and C. E. Wieman, Formation of Bright Matter-Wave Solitons during the Collapse of Attractive Bose-Einstein Condensates, Phys. Rev. Lett. **96**, 170401 (2006).
[45] E. A. Donley, N. R. Claussen, S. L. Cornish, J. L. Roberts, E. A. Cornell, and C. E. Wieman, Dynamics of collapsing and exploding Bose-Einstein condensates, Nature (London) **412**, 295 (2001).
[46] N. Akhmediev and V. I. Korneev, Modulation instability and periodic solutions of the nonlinear Schrödinger equation, Theor. Math. Phys. **69**, 1089 (1986).
[47] N. Devine, A. Ankiewicz, G. Genty, J. M. Dudley, and N. Akhmediev, Recurrence phase shift in Fermi-Pasta-Ulam nonlinear dynamics, Phys. Lett. A **375**, 4158 (2011).
[48] N. V. Vitanov, Transition times in the Landau-Zener model, Phys. Rev. A **59**, 988 (1999).
[49] K. Mullen, E. Ben-Jacob, Y. Gefen, and Z. Schuss, Time of Zener Tunneling, Phys. Rev. Lett. **62**, 2543 (1989).
[50] Q. Niu and M. G. Raizen, How Landau-Zener Tunneling Takes Time, Phys. Rev. Lett. **80**, 3491 (1998).
[51] X. Z. Liu, D. P. Tian, and B. Chong, Transition time of nonlinear Landau-Zener model in adiabatic limit, Mod. Phys. Lett. B **30**, 1650194 (2016).
[52] Q. Park and H. J. Shin, Painlevé analysis of the coupled nonlinear Schrödinger equation for polarized optical waves in an isotropic medium, Phys. Rev. E **59**, 2373 (1999).
[53] J. M. Dudley, F. Dias, M. Erkintalo, and G. Genty, Instabilities, breathers and rogue waves in optics, Nat. Photonics **8**, 755 (2014).
[54] K. Hammani, B. Wetzel, B. Kibler, J. Fatome, C. Finot, G. Millot, N. Akhmediev, and J. M. Dudley, Spectral dynamics of modulation instability described using Akhmediev breather theory, Opt. Lett. **36**, 2140 (2011).
[55] V. E. Zakharov and L. A. Ostrovsky, Modulation instability: The beginning, Phys. D (Amsterdam, Neth.) **238**, 540 (2009).
[56] T. Hansson, D. Modotto, and S. Wabnitz, Dynamics of the modulational instability in microresonator frequency combs, Phys. Rev. A **88**, 023819 (2013).

[57] L.-C. Zhao and L. Ling, Quantitative relations between modulational instability and several well-known nonlinear excitations, J. Opt. Soc. Am. B **33**, 850 (2016).

[58] M. Erkintalo, K. Hammani, B. Kibler, C. Finot, N. Akhmediev, J. M. Dudley, and G. Genty, Higher-Order Modulation Instability in Nonlinear Fiber Optics, Phys. Rev. Lett. **107**, 253901 (2011).

[59] S. Wabnitz and N. Akhmediev, Efficient modulation frequency doubling by induced modulation instability, Opt. Commun. **283**, 1152 (2010).

[60] F. D. Zong, Y. S. Yan, and S. T. Shen, Higher-order modes of modulation instability in Bose-Einstein condensates with a time-dependent three-dimensional parabolic potential, J. Phys. Soc. Jpn. **83**, 104002 (2014).

[61] B. Frisquet, B. Kibler, and G. Millot, Collision of Akhmediev Breathers in Nonlinear Fiber Optics, Phys. Rev. X **3**, 041032 (2013).

[62] M. Erkintalo, G. Genty, B. Wetzel, and J. M. Dudley, Akhmediev breather evolution in optical fiber for realistic initial conditions, Phys. Lett. A **375**, 2029 (2011).

[63] T. M. Bersano, V. Gokhroo, M. A. Khamehchi, J. D'Ambroise, D. J. Frantzeskakis, P. Engels, and P. G. Kevrekidis, Three-Component Soliton States in Spinor $F = 1$ Bose-Einstein Condensates, Phys. Rev. Lett. **120**, 063202 (2018).

[64] T. Köhler, K. Góral, and P. S. Julienne, Production of cold molecules via magnetically tunable Feshbach resonances, Rev. Mod. Phys. **78**, 1311 (2006).

[65] C. Chin, R. Grimm, P. Julienne, and E. Tiesinga, Feshbach resonances in ultracold gases, Rev. Mod. Phys. **82**, 1225 (2010).

[66] M. Olshanii, Atomic Scattering in the Presence of an External Confinement and a Gas of Impenetrable Bosons, Phys. Rev. Lett. **81**, 938 (1998).

[67] D. Luo, Y. Jin, J. H. V. Nguyen, B. A. Malomed, O. V. Marchukov, V. A. Yurovsky, V. Dunjko, M. Olshanii, and R. G. Hulet, Creation and Characterization of Matter-Wave Breathers, Phys. Rev. Lett. **125**, 183902 (2020).

[68] R. Grimm, M. Weidemüller, and Y. B. Ovchinnikov, Optical dipole traps for neutral atoms, Adv. At. Mol. Opt. Phys. **42**, 95 (2000).

[69] L.-C. Zhao, L.-Z. Meng, Y.-H. Qin, Z.-Y. Yang, and J. Liu, Topological vector potentials underlying one-dimensional nonlinear waves, arXiv:2102.10914.